Fiber Nonlinearity Limitations in Ultra-Dense WDM Systems

Mingchia Wu and Winston I. Way, *Fellow, IEEE*

***Abstract*—Transmission performance of ultra-dense 2.5- and 10-Gb/s nonreturn-to-zero intensity-modulated direct-detection wavelength-division-multiplexing systems in various single-mode fibers is investigated. Fundamental limiting factors and their remedies by using optimum dispersion compensation for periodically amplified systems in C band are presented.**

***Index Terms*—Cross-phase modulation (XPM), dense-wavelength-division multiplexing (DWDM), fiber nonlinearity, four-wave mixing (FWM), self-phase modulation (SPM).**

I. Introduction

In order to increase the transmission capacity of a dense-wavelength-division-multiplexing (DWDM) optical system, one can either increase the transmission data rate per wavelength or increase the number of wavelengths while keeping proper transmission granularity. The first approach can be illustrated by the recent increase in data rate per wavelength from 2.5 to 10 and 40 Gb/s. The second approach is to significantly increase the number of wavelengths in a fixed optical spectrum (e.g., C band) by decreasing the spacing between neighboring wavelengths. By using this approach, a capacity increase can be achieved without resorting to high-speed (e.g., >40-Gb/s) electronics, while keeping compatibility with existing 2.5/10-Gb/s synchronous optical network/synchronous digital hierarchy (SONET/SDH) equipment. Along this line, the focus of this paper is on ultra-dense-wavelength-division-multiplexing (U-DWDM) transmission systems. Examples of U-DWDM systems include 25-GHz-spaced 10-Gb/s and 6.25-GHz-spaced 2.5-Gb/s transmission systems.

It should be noted that, even though a few U-DWDM system experiments have been carried out recently [1]–[5], the fundamental limiting factors and their remedies in such systems remain unclear. It is obvious that there are different transmission issues to be dealt with in the previously mentioned two distinct approaches. When the transmitting data rate is higher than 40 Gb/s, severe chromatic dispersion and polarization-mode dispersion problems will have to be resolved even before dealing with optical nononlinearity-induced penalties. On the other hand, U-DWDM systems intuitively should have optical-nonlinearity-induced system limitations such as four-wave mixing (FWM) and cross-phase modulation (XPM) penalties. This study considers various nonlinear distortions/interferences to determine the fiber nonlinearity limited maximum transmission distances in U-DWDM systems. The optimum launched power, the dispersion compensation ratio (DCR), and the dominant optical nonlinearities in different systems are also discussed.

In Section II, the paper provides an overview of the main nonlinear distortions/interferences in U-DWDM systems. Section III analytically calculates and numerically simulates the capacity and distance limitations of U-DWDM systems. Discussions and conclusions are provided in Sections IV and V, respectively.

II. Fundamental Limiting Factors in U-DWDM Systems

The three fundamental limiting factors in U-DWDM systems include

1) various random noise terms;
2) fiber chromatic dispersion-induced intersymbol interference (ISI);
3) optical-nonlinearity-induced distortion and interference.

All three factors are common to conventional DWDM systems, although the third factor can be unique in the case of extremely close channel spacing.

We assume a multisegmented, optically amplified U-DWDM system as shown in Fig. 1(a) to derive the general forms of fiber nonlinearity-induced interferences/distortions. The transmitter side contains M externally modulated light sources at wavelength λ_i, where $i = 1, 2, \ldots, M$. The M wavelengths are nonreturn-to-zero (NRZ) modulated with independent data pattern and are multiplexed and demultiplexed by either a pair of ideal multiplexers and demultiplexers or by a pair of broad-band couplers (with an ideal filter in each receiver). A tunable postdispersion compensator (PDC), which can be tuned up to -2000 ps/nm, is located right before each optical receiver to optimize the received signal performance of each individual channel. The nth segment contains a span $L^{(n)}$ of fiber and an erbium-doped optical amplifier with a noise figure of 5 dB and a power gain $g^{(n)} = \exp(\alpha^{(n)} L^{(n)})$ to compensate the fiber loss. The fiber can be single-mode fibers (SMFs), nonzero-dispersion-shifted fibers (NZDSFs), or dispersion compensation fibers (DCFs) used for broad-band dispersion compensation. Fiber parameters assumed for analysis and numerical simulations throughout this paper are summarized in Table I. When DCFs are used in a transmission link, their additional loss must be compensated by additional stages of optical amplifiers. In this case, we use a system configuration shown in Fig. 1(b), which can be considered a special case of Fig. 1(a). Note that in Fig. 1(b), each amplifier stage comprises a span of SMF (or NZDSF), an optical amplifier to compensate the fiber

Manuscript received May 27, 2003; revised January 19, 2004.

M. Wu is with the Department of Communications Engineering, National Chiao-Tung University, Hsinchu 300, Taiwan, R.O.C.

W. I. Way is with OpVista Inc., Irvine, CA 92618, USA.

Digital Object Identifier 10.1109/JLT.2004.829222

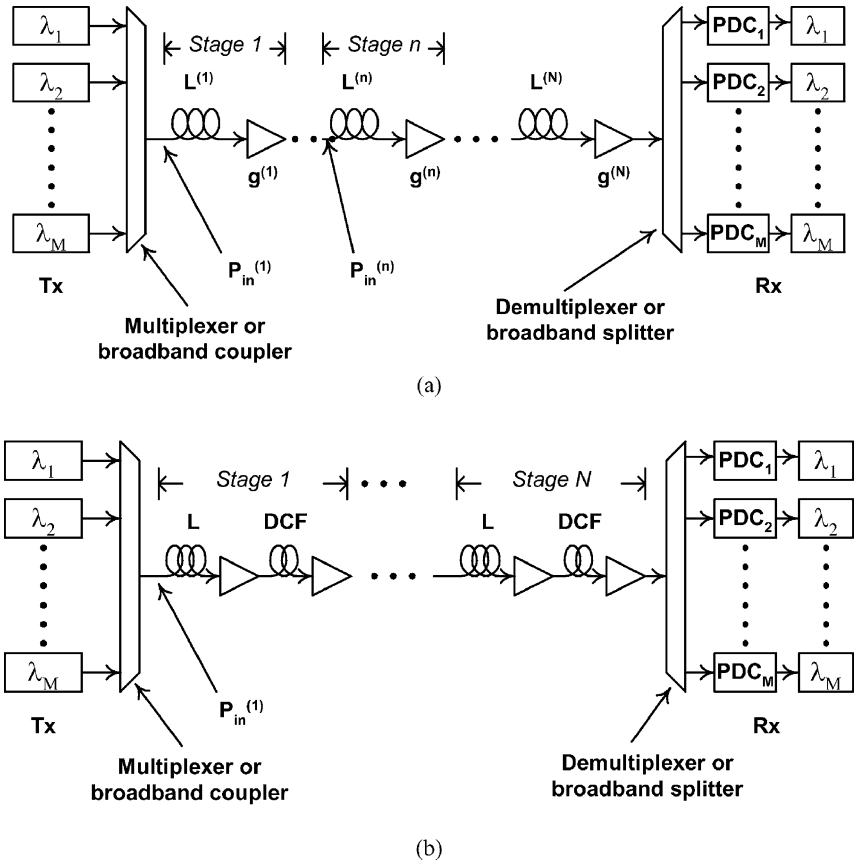

Fig. 1. (a) General U-DWDM system model. (b) Periodically amplified U-DWDM system model with postdispersion compensation in every amplifier stage.

loss, a span of DCF whose span length is determined by the designed DCR, and another optical amplifier to compensate for the DCF loss. Therefore, it is equivalent to having a total of $2N$ stages in the general system model shown in Fig. 1(a). We will use this periodically amplified and dispersion-compensated system model to analyze the optimum design of U-DWDM systems in Section III.

Throughout this paper, we will use $Q^2 = 15.6$ dB (which gives BER $= 10^{-9}$ under the assumption of Gaussian distributed noise) as the minimum system performance requirement. Q^2 follows the conventional Q^2 definition and is given by

$$Q^2(\text{dB}) = 20\log_{10}\left(\frac{m_1 - m_0}{\sigma_1 + \sigma_0}\right) \tag{1}$$

where m_i and σ_i are the mean and standard deviation values for mark ($i = 1$) and space ($i = 0$), respectively. This system requirement assures error-free transmission when typical forward-error correction (FEC) encoders/decoders are added. It should be noted that although many published analytical results showed that nonlinear distortions or interference are usually non-Gaussian distributed, they did show that under small optical-nonlinearity penalties, Gaussian approximation can serve as an upper bound and can be viewed as a good approximation [6], [7]. As will be seen subsequently in our analysis, fiber nonlinearity-induced distortions/interference is assumed to be of the same order of magnitude as amplified spontaneous emission (ASE) noise, and at $Q^2 = 15.6$ dB, it can be considered small enough to be approximated as random noise just as ASE noise. Note that the optical-signal-to-noise ratio (OSNR) [8], [9] is not used as a performance index in our study. This is because XPM and self-phase-modulation (SPM) are not measurable in the optical domain unless they are converted to electrical signal at a photodetector.

TABLE I
FIBER PARAMETER ASSUMPTIONS

	SMF	NZDSF	DCF
Chromatic Dispersion, D(ps/nm/km)	16-18	2-6	-85
Effective core area, A_{eff}(μ m^2)	85	72	21
Nonlinear refractive index, n_2(m^2/W)	2.5×10^{-20}	2.5×10^{-20}	2.5×10^{-20}
Attenuation, α (dB/km)	0.2	0.2	0.4
Dispersion Slope @1545nm (ps/nm^2/km)	0.058	0.11	-

The nonlinear interferences/distortions under consideration typically occur at mark, and thus $\sigma_1^2 \gg \sigma_0^2$. The standard deviation σ_1 in (1) is modeled as

$$\sigma_1^2 = \sigma_{\text{ASE},1}^2 + \sigma_{\text{NL},1}^2 \tag{2}$$

where $\sigma_{\text{ASE},1}^2$ is the noise variance due to optical amplifiers and is dominated by signal–spontaneous emission beat noise at the

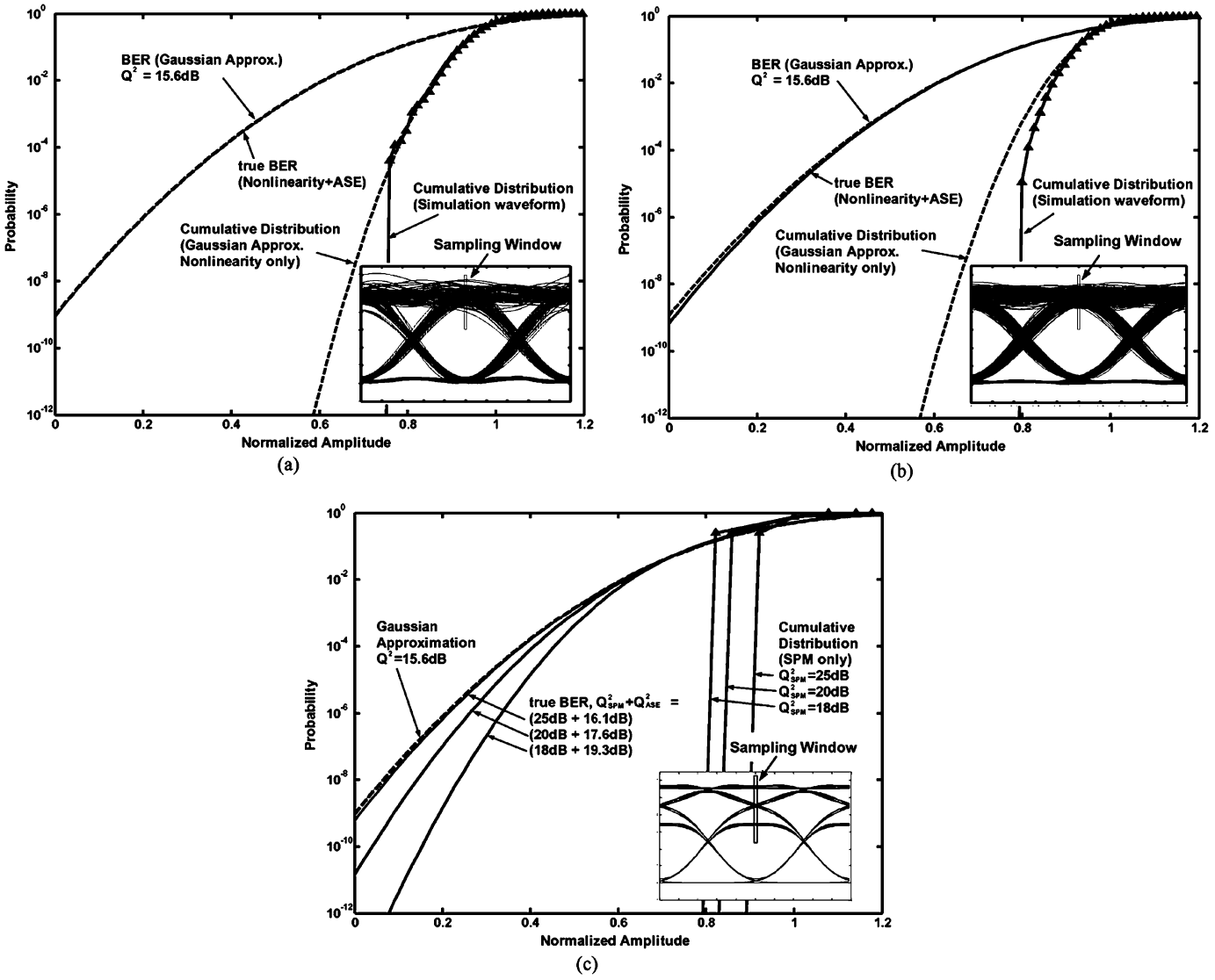

Fig. 2. Cumulative waveform amplitude distribution of simulated nonlinear interference/distortion obtained at an optimum sampling point for the central four channels of a 40-ch U-DWDM system. The result is a distribution of 50 independent simulations. Dashed curves are Gaussian approximation. (a) (FWM-dominant) 2.5-Gb/s/6.25-GHz system after 5400-km SMF transmission, corresponding to the 40-km span, DCR $= 93\%$ point in Fig. 6(a). 51 200 symbols, $Q^2 = 21.5$ dB. (b) (SPM, XPM-dominant) 10-Gb/s/25-GHz system after 4000-km NZDSF ($D = 6$ ps/nm/km), corresponding to the 40-km span, DCR $= 90\%$ point in Fig. 10(a). 204 800 symbols, $Q^2 = 21$ dB. (c) (SPM-dominant) comparison between Gaussian approximation and the true distribution. The true BERs (solid curves) are obtained by using the method given in the Appendix .

presence of mark. $\sigma^2_{\mathrm{NL},1} = \sigma^2_{\mathrm{FWM},1} + \sigma^2_{\mathrm{XPM},1} + \sigma^2_{\mathrm{SPM},1}$ is the interference/distortion variance due to fiber nonlinearities, including FWM, XPM, and SPM. Note that although SPM induces deterministic waveform distortion, we approximate it as a normal variance term $\sigma^2_{\mathrm{SPM},1}$ because 1) we want to compare the effect of SPM with that of FWM and XPM across various DCR, distances, fibers, and data rates by using the same parameter and 2) in cases where SPM distortion has the same order of magnitude as FWM/XPM interference, it is difficult to separate deterministic distortion from random interference in numerical simulations. The range of validity for this approximation is shown in Fig. 2.

Note that space level impairment is dominated by deterministic distortions due to linear dispersion. Spontaneous–spontaneous emission beat noise and nonlinearity are negligible at space level. Space-level deterministic distortion is taken into account in our calculations and simulations by replacing m_0 in (1) with the highest distorted space amplitude. Therefore, the effect of linear-dispersion-induced ISI on (1) is to effectively introduce additional eye-opening penalties (EOPs).

To verify the validity of treating optical nonlinearities as random noise in (2), under the conditions of a relatively large Q^2 and the fact that the variance of these impairments are smaller than that of ASE, Fig. 2 shows the amplitude distributions of mark of simulation data at the optimum decision point of received eye diagrams. Fig. 2(a) shows the amplitude distribution in a 40-ch 2.5-Gb/s/6.25-GHz system transmitted over a 5400-km SMF with DCR $= 93\%$ [corresponding to the point shown in Fig. 6(a)]. The result is a distribution of 51 200 symbols, which were obtained from the central four channels (256 symbols per channel) and 50 independent simulations. The average Q^2 is 21.5 dB and is dominated by FWM. Dashed

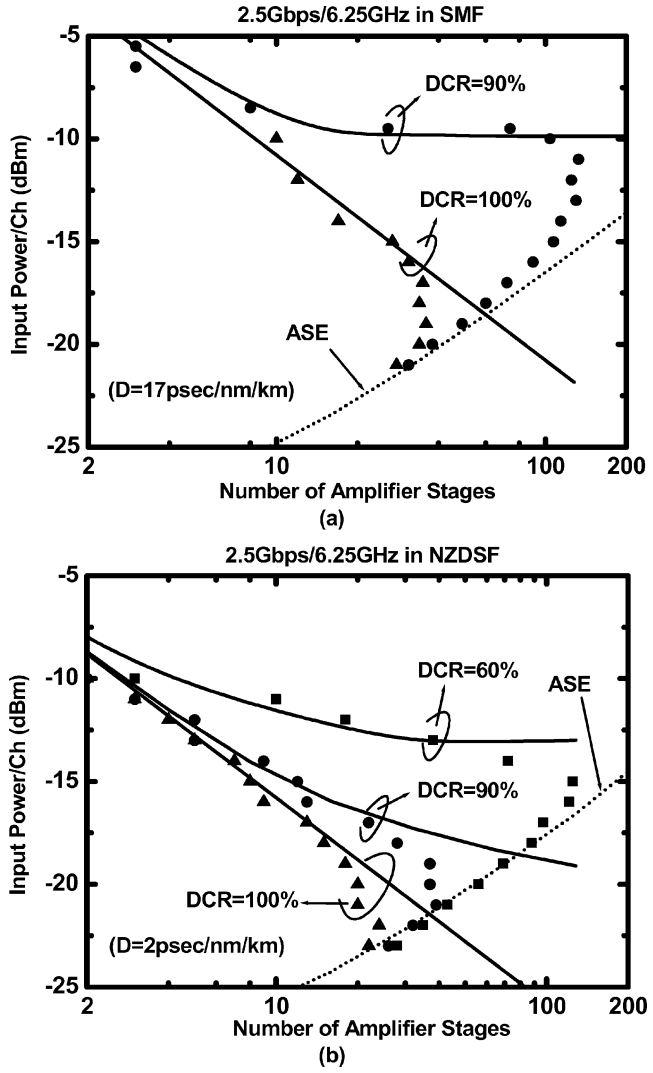

Fig. 3. FWM- and ASE-limited maximum fiber input power per channel of 2.5-Gb/s/6.25-GHz systems as a function of amplifier stages for different DCRs in (a) SMF and (b) NZDSF. Assume 40 km per amplifier stage. Dotted curve is ASE noise-limited minimum input power. Symbols are simulation results.

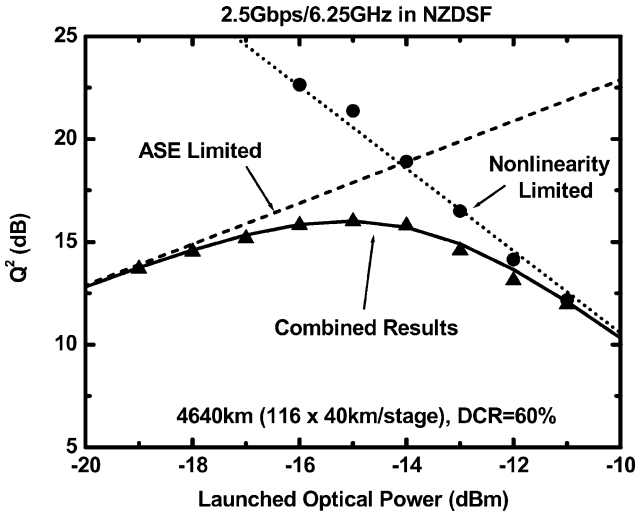

Fig. 4. Q^2 as a function of average launched optical power of a 2.5-Gb/s/6.25-GHz system after 4640-km NZDSF, which corresponds to the maximum transmission point of Fig. 5(a). Solid curve and circles are calculated and simulated received Q^2, respectively. Dotted line represents the optical-nonlinearity-limited Q^2. Dashed line is ASE-limited Q^2. Solid triangles are the combined results of ASE and fiber nonlinearity.

curves are Gaussian approximations with the same Q^2. We can see that the FWM amplitude distribution matches very well with the Gaussian approximation. This is because the dominant interference is contributed from many different independent channels via FWM. Because of finite U-DWDM channels and simulation symbols, the cumulative distribution of the simulated waveform (excluding ASE noise) deviates away from Gaussian approximation at the tail. However, when ASE noise is added, the true BER (solid curve, with the cumulative distribution calculated based on a method detailed in the Appendix [7], [10]) and a BER with Gaussian approximation (dashed curve) match each other extremely well. Fig. 2(b) shows the amplitude distribution in a 40-ch 10-Gb/s/25-GHz system transmitted over a 4000-km NZDSF with 6-ps/nm/km fiber dispersion and DCR $= 93\%$ [corresponding to the maximum transmission distance in Fig. 10(a)]. The result is a distribution of 204 800 symbols, which were obtained from the central four channels (1024 symbols per channel) and 50 independent simulations. The average Q^2 is 21 dB and is dominated by SPM and XPM [see Fig. 10(b)]. Although a slight deviation from Gaussian distribution is observed, the distribution can be brought closer to Gaussian when ASE noise is added [see the cumulative distribution (BER) curve with ASE noise included]. Noise and nonlinearities on space level are neglected and not shown in these figures. Fig. 2(c) shows the amplitude distribution when SPM-induced waveform distortion is the dominant impairment. We checked an extreme case in which the mark level is split into three levels due to SPM [see the eye diagram shown in the inset of Fig. 2(c)]. We assume the three levels are binomially distributed with probabilities of 1/4, 1/2, and 1/4, representing the probabilities of bit sequences "00", "10" or "01", and "11", respectively. Because SPM results in deterministic waveform distortion, they cannot be approximated as Gaussian noise. However, when ASE noise with the same order of magnitude is added, the situation is different. The true BERs (solid curves) are obtained with a method detailed in the Appendix. The Gaussian approximation by treating SPM as a normal variance in (2) is shown as the dotted curve. Three different values of $Q^2_{\rm SPM}$, 18, 20, and 25 dB, are shown in the figure. The corresponding $Q^2_{\rm ASE}$ are chosen so that the combined $Q^2_{\rm SPM+ASE} = 15.6$ dB. We can see that, although a large deviation between Gaussian approximation and the true BER occurs when $Q^2_{\rm SPM} < Q^2_{\rm ASE}$, Gaussian approximation matches very well with the corresponding true BER when $Q^2_{\rm SPM} > 25$ dB. As we will see the in Section III (Figs. 10 and 11), $Q^2_{\rm SPM} > 25$ dB is generally satisfied in our calculations/simulations, especially in the region near the optimum DCR.

In the following, we will concentrate on analytical tools for each individual fiber-nonlinearity-induced interference or distortion and linear-dispersion-induced ISI. In Section III, we will add amplifier noise in the overall system performance evaluation.

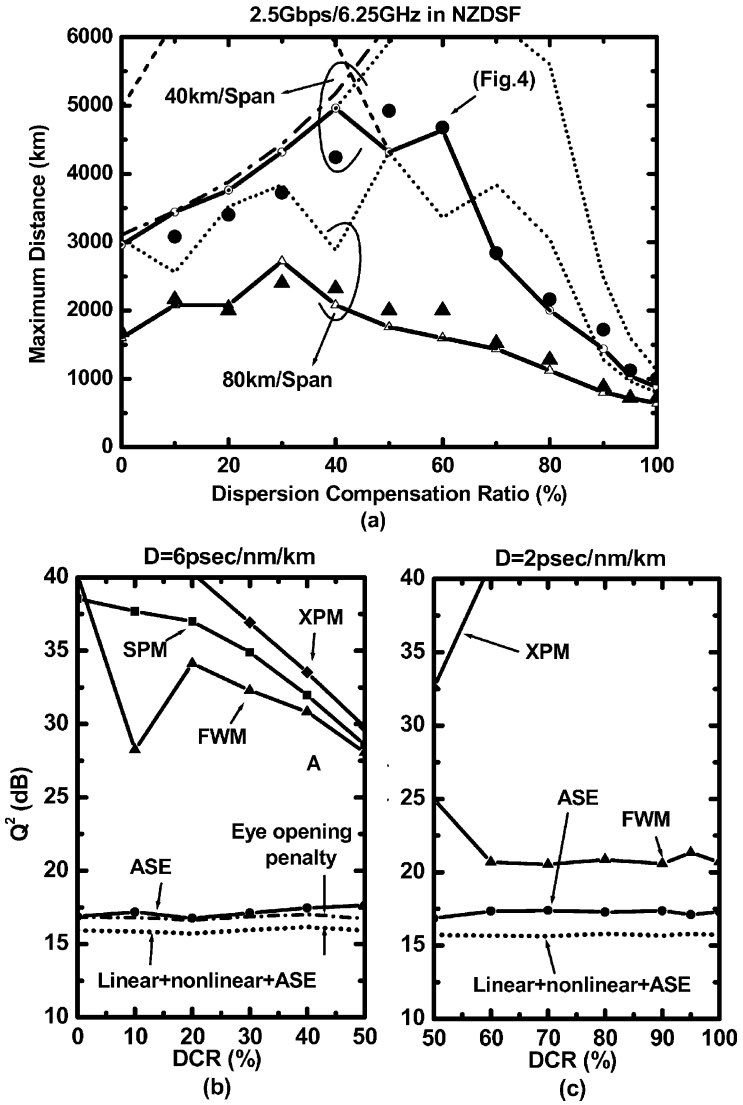

Fig. 5. (a) Calculated and simulated ASE-, fiber linear-dispersion-, and nonlinearity-limited maximum transmission distance of 2.5-Gb/s/6.25-GHz-spaced systems ($Q^2 \geqq 15.6$ dB) as a function of inline DCR in NZDSF. Results for both 40- and 80-km fiber spans are shown. Dashed and dotted curves were calculated based on $D = 2$ and 6 ps/nm/km, respectively, while solid curves represent the worse of the two. • and ▲ are simulation results. Inline DCFs are used for dispersion compensation, and the input power into DCF is 3 dB lower than that into transmission fiber. A tunable PDC (up to -2000 ps/nm) was used to optimize the individual channel performance. The dashed–dotted curve is the linear-dispersion limitation at $D = 6$ ps/nm/km. (b) and (c) Calculated individual Q^2 for 40-km fiber span.

A. Four-Wave Mixing

In an amplified and dispersion-compensated DWDM system, FWM terms generated at every amplifier stage are added according to their phase relations. Starting from the coupled nonlinear Schrödinger's equations (NLSEs) with three continuous-wave (CW) wavelengths located in f_i, f_j, and f_k and applying the general system model as shown in Fig. 1(a), we can get a general form of FWM in E-field at a frequency $f_{\mathrm{FWM}} = f_i + f_j - f_k$ and a distance $L_T = \sum_{n=1}^{N} L^{(n)}$ [6], [11]–[13]. See (3) shown at the bottom of the page, where $|E_{\mathrm{FWM},ijk}(L_T)|^2 = P_{\mathrm{FWM},ijk}(L_T)$ is the FWM power; $|E_{i,j,k}|^2 = P_{i,j,k}$ is the launched CW signal power at frequencies $f_{i,j,k}$; d is the degeneracy factor ($d = 1$ for

$$
\begin{aligned}
&E_{\mathrm{FWM},ijk}(L_T) \\
&= d \cdot E_i E_j E_k^* \\
&\cdot \sum_{n=1}^{N} \left\{ \gamma^{(n)} \exp\left[-\sum_{\ell=1}^{n} \frac{\alpha^{(\ell)}}{2} L^{(\ell)} \right] \prod_{\ell=1}^{n} \sqrt{g^{(\ell)}}^3 \cdot \exp\left[\sum_{\ell=1}^{n-1} \left(-\alpha^{(\ell)} L^{(\ell)} + i\Delta\beta^{(\ell)} L^{(\ell)} \right) \right] \cdot \left[\frac{\exp\left(-\alpha^{(n)} L^{(n)} + i\Delta\beta^{(n)} L^{(n)} \right) - 1}{-\alpha^{(n)} + i\Delta\beta^{(n)}} \right] \right\}.
\end{aligned}
\tag{3}
$$

$i = j$ and $d = 2$ for $i \neq j$); $\gamma_i^{(n)} = 2\pi n_2^{(n)}/\lambda A_{\text{eff}}^{(n)}$ is the fiber nonlinearity parameter in the nth fiber section; and $\Delta\beta^{(n)}$ represents the phase mismatch at nth fiber section and may be expressed in terms of signal frequency differences as

$$\Delta\beta^{(n)} = \frac{2\pi\lambda^2}{c}\,|f_i - f_k|\,|f_j - f_k| \cdot \left\{ D^{(n)} + \frac{\lambda^2}{2c} \cdot \frac{dD^{(n)}}{d\lambda}\left(|f_i - f_k| + |f_j - f_k|\right)\right\}. \quad (4)$$

In general, the dispersion-slope term can be neglected in nonzero-dispersion regions; for example, the second term due to dispersion slope in the C band is only 0.022 ps/nm/km for 25-GHz spacing in NZDSF, which is much smaller than typical $D = 2$ to 6 ps/nm/km. For periodically amplified systems without dispersion compensation, (3) can be simplified to the result given in [11] by setting $\alpha^{(n)} = \alpha$, $L^{(n)} = L$, $g^{(n)} = e^{\alpha L}$, and $\Delta\beta^{(n)} = \Delta\beta$ for all n, such that

$$P_{\text{FWM},ijk}(N \cdot L) = \eta_{ijk}\gamma^2 d^2 L_{\text{eff}}^2 P_i P_j P_k \cdot e^{-\alpha L} \cdot \frac{\sin^2\left(\frac{N\Delta\beta_{ijk}\Delta L}{2}\right)}{\sin^2\left(\frac{\Delta\beta_{ijk}\Delta L}{2}\right)} \quad (5)$$

where $L_{\text{eff}} = \{1 - \exp(-\alpha L)\}/\alpha$ is the effective length, and η_{ijk} is the mixing efficiency given by

$$\eta_{ijk} = \frac{\alpha^2}{\alpha^2 + \Delta\beta^2}\left[1 + 4e^{-\alpha L} \cdot \frac{\sin^2\left(\frac{\Delta\beta L}{2}\right)}{\left(1 - e^{-\alpha L}\right)^2}\right]. \quad (6)$$

For systems with dispersion compensation, the accumulated phase term $\exp\left[\sum_{\ell=1}^{n-1}\left(i\Delta\beta^{(\ell)}L^{(\ell)}\right)\right]$ in (3) represents the phase relation among FWM terms generated in each amplifier stage and is proportional to fiber dispersion, channel spacing, and fiber length. For conventional DWDM systems in nonzero-dispersion fibers, where $\Delta\beta^{(\ell)}$ is large (e.g., $\Delta\beta^{(\ell)} \approx 2$ rad/km for a 100-GHz-spaced DWDM system in NZDSF), small variation in span length $L^{(\ell)}$ can result in large phase variation in FWM terms. Therefore, $\exp\left[\sum_{\ell=1}^{n-1}\left(i\Delta\beta^{(\ell)}L^{(\ell)}\right)\right]$ was sometimes assumed to be randomly distributed over $[0, 2\pi]$ and the FWM terms generated in different fiber spans are statistically power added regardless of the phase relation among stages, and the resultant FWM power is proportional to N [14]. This assumption, however, is not valid for U-DWDM systems, especially in the case of analyzing optimum DCR. For example, consider a 6.25-GHz-spaced U-DWDM systems in NZDSF, $\Delta\beta^{(\ell)} \approx 0.008$ rad/km; therefore, small variations on $L^{(\ell)}$ have a negligible effect on $\exp\left[\sum_{\ell=1}^{n-1}\left(i\Delta\beta^{(\ell)}L^{(\ell)}\right)\right]$. As a result, random variable assumption is not valid, and we need to use the exact form in (3), where the FWM terms generated in different fiber spans are added in the E-field.

Note that the above analysis is based on three CW optical carriers without modulations. In an M-channel NRZ-modulated U-DWDM system, the total FWM at a certain channel with frequency $f_S = f_{\text{FWM}}$ is expressed as the sum of all the FWM terms with $f_{\text{FWM}} = f_i + f_j - f_k$ in E-field [6]

$$E_{\text{FWM}} = \sum_{f_i+f_j-f_k=f_{\text{FWM}}} b_i b_j b_k \sqrt{P_{\text{FWM},ijk}}\, e^{j\theta_{ijk}} \quad (7)$$

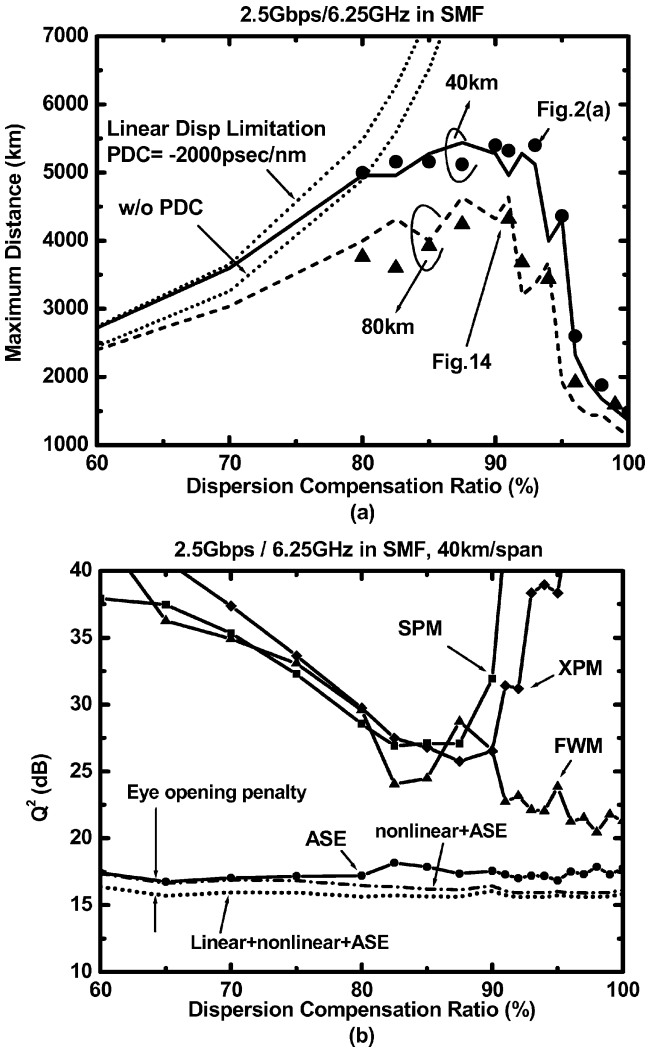

Fig. 6. (a) Calculated and simulated ASE-, fiber linear-dispersion-, and nonlinearity-limited maximum transmission distance of 2.5-Gb/s/6.25-GHz-spaced systems ($Q^2 \geqq 15.6$ dB) as a function of in-ine DCR in SMF. Results for both 40- and 80-km fiber spans are shown. • and ▲ are simulation results. Inline DCFs are used for dispersion compensation, and the input power into DCF is 3 dB lower than that into transmission fiber. A tunable PDC (up to -2000 ps/nm) was used to optimize the individual channel performance. (b) Calculated individual Q^2 for 40-km fiber span.

where $b_{i,j,k} = 1$ or 0, depending on whether the i, j, kth channel is mark or space. θ_{ijk} is the random phase of FWM terms. If the wavelengths in a U-DWDM system are equally spaced, some FWM terms will fall right below other signal bands. At the receiver, the interference on mark is originated from the beating between signal and FWM after a photodiode. The interference on space is originated from the beating between FWM terms (similar to spontaneous–spontaneous emission beat noise) and can usually be neglected in the signal-to-noise ratio (SNR) range of interest. The exact probability density functions of the FWM interference on both mark and space are detailed in [6]. It was shown in [6] that the Gaussian distribution can serve as a good approximation and the equivalent Q factor due to FWM can be written as

$$Q_{\text{FWM}}^2\,(\text{dB}) = 10\log_{10}\left(\frac{\frac{1}{2}P_S}{\overline{P}_{\text{FWM}}}\right) \quad (8)$$

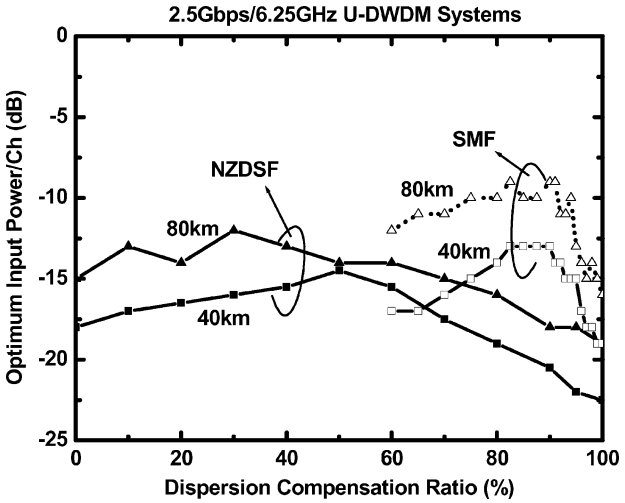

Fig. 7. Optimum launched power per channel as a function of DCR in 2.5-Gb/s/6.25-GHz systems. The symbols correspond to the maximum transmission distances at different DCR in Figs. 5(a) and 6(a).

where P_S is the peak received signal power per channel. $\overline{P}_{\rm FWM} = \left\langle |E_{\rm FWM}|^2 \right\rangle$ can be written as [6]

$$\begin{aligned}\overline{P}_{\rm FWM} =& \frac{1}{8} \sum_{f_i \neq f_j \neq f_k \neq f_{\rm FWM}} P_{{\rm FWM},ijk} \\ &+ \frac{1}{4} \sum_{f_i \neq f_j \neq f_k = f_{\rm FWM}} P_{{\rm FWM},ijk} \\ &+ \frac{1}{4} \sum_{f_i = f_j \neq f_k} P_{{\rm FWM},ijk} \end{aligned} \quad (9)$$

where the three fractional numbers represent the probabilities of coexisting marks among the four wavelengths (including the signal channel itself). Note that in a U-DWDM system with equal launched power per channel, $\overline{P}_{\rm FWM} \propto P_S^3$. Therefore, according to (8), $Q_{\rm FWM}^2 \propto 1/P_S^2$.

It is a time-consuming task to calculate all the FWM terms in (9) because the number of FWM terms is proportional to the cubic of channel numbers M^3. However, a strong phase matching among the four wavelengths (f_i, f_j, f_j, and $f_{\rm FWM}$) is required for the new FWM term to build up and was reflected in the FWM efficiency (6). Note that (6) has low-pass characteristics with a -3-dB point at $\Delta f = \sqrt{\alpha(c/2\pi\lambda^2 D)}$, e.g., the 3-dB points are about 7.3 GHz and 21.2 GHz for $D = 17$ and 2 ps/nm/km, respectively. This means that 1) for a U-DWDM with channel spacing close to 7.3/21.2 GHz in SMF/NZDSF fibers, FWM would become very severe and 2) when calculating or simulating the penalty due to FWM in a U-DWDM system with a large channel count, a smaller number of closely spaced channels can possibly be used to obtain the final results (with the contribution from farther away channels neglected). Using (9), we find that for a 6.25-GHz channel spacing in a transmission fiber with D as low as 2 ps/nm/km, the difference of FWM power is increased by less than 1 dB when the number of channels under consideration is increased from 40 to 640 channels (fully loaded C band). The difference is even smaller when considering SMF and larger channel spacing. Therefore, in the following analysis and numerical simulations, only up to 40 channels are used. This could save considerable computer time in Section III.

B. Cross-Phase Modulation

The XPM-induced phase-modulation-to-intensity-modulation (PM-to-IM) interference was analyzed in frequency domain by using a modulated pump channel k and a CW probe channel s and can be written as [15], [16]

$$\widetilde{P}_{{\rm XPM},sk}(L_T,\omega) = P_s(L_T) \cdot \widetilde{P}_k(0,\omega) \cdot H_{sk}^{\rm XPM}(L_T,\omega) \quad (10)$$

where $P_s(L_T)$ is the optical power of a CW channel at a distance L_T, $\widetilde{P}_k(0,\omega)$ is the Fourier transform of the modulated pump channel, $\widetilde{P}_k(0,\omega) = \int_{-\infty}^{\infty} P_k(0,t) \cdot e^{-j\omega t} dt$, and $H_{sk}^{XPM}(L_T,\omega)$ is the normalized frequency response of the XPM-induced intensity modulation from channel k to channel s and can be written as [15]. See (11) shown at the bottom of the page, where N is the stage number in Fig. 1(a), $a_{sk}^{(n)} = \alpha^{(n)} - j\omega d_{sk}^{(n)}$, $b_s^{(n)} = \omega^2 D_s^{(n)} \lambda_s^2/4\pi c$, and $B_s^{(n)} = \omega^2 \lambda_s^2/4\pi c \sum_{\ell=n+1}^{N} D_s^{(\ell)} L^{(\ell)}$. $d_{sk}^{(n)} = \left(v_{gs}^{(n)}\right)^{-1} - \left(v_{gk}^{(n)}\right)^{-1} \approx D \cdot \lambda^2/c \cdot |s-k| \cdot \Delta f$ is the walk-off parameter between channels s and k, $v_{gs}^{(n)}$ is the group velocity of channel s in the nth fiber span, and Δf is the frequency spacing between adjacent channels. The XPM induced interference in channel s in a digitally modulated U-DWDM system can be written as

$$\begin{aligned}&\hat{P}_{{\rm XPM},s}(L_T,t) \\ &= \hat{P}_s(L_T,t) \cdot \frac{1}{2\pi} \cdot \sum_{k \neq s} \int_{-B_e}^{B_e} \widetilde{P}_k(0,\omega) H_{sk}^{\rm XPM}(\omega) e^{j\omega t} d\omega \end{aligned} \quad (12)$$

$$\begin{aligned}&H_{sk}^{\rm XPM}(L_T,\omega) \\ &= \sum_{n=1}^{N} \left\{ \gamma_s^{(n)} \prod_{\ell=1}^{n-1} g_s^{(\ell)} \cdot \exp\left[\sum_{\ell=1}^{n-1} \left(-\alpha^{(\ell)} L^{(\ell)} + j d_{sk}^{(\ell)} \omega L^{(\ell)} \right) \right] \right. \\ &\left. \cdot \frac{4}{\left(a_{sk}^{(n)}\right)^2 + \left(b_s^{(n)}\right)^2} \left[a_{sk}^{(n)} \sin\left(B_s^{(n-1)}\right) - b_s^{(n)} \cos\left(B_s^{(n-1)}\right) + \left[a_{sk}^{(n)} \sin\left(-B_s^{(n)}\right) - b_s^{(n)} \cos\left(B_s^{(n)}\right) \right] \exp\left(-a_{sk}^{(n)} L^{(n)}\right) \right] \right\} \end{aligned} \quad (11)$$

where $\hat{P}_s(L_T,t)$ is the optical waveform due to residual linear dispersion at a distance L_T and is given by [16]

$$\hat{P}_s(L_T,t)=\frac{1}{2\pi}\cdot\int_{-\infty}^{\infty}\widetilde{P}_s(0,\omega)\cdot\cos\left(\frac{\omega^2\lambda^2}{4\pi c}\left(\sum_{n=1}^{N}D^{(n)}L^{(n)}-\text{PDC}\right)\right)e^{j\omega t}d\omega \quad (13)$$

where $\widetilde{P}_s(0,\omega)$ is the Fourier transform of the launched intensity waveform of channel s. This general form can be used to analyze arbitrary modulation format, DCR, and PDC. We can see that the DC term of XPM-induced interference in (11) is zero, and the total variance of the XPM-induced interference in channel s of a U-DWDM system can be obtained by summing all the variances as

$$\begin{aligned}\sigma^2_{\text{XPM},s}&=\sum_{k\neq s}\sigma^2_{\text{XPM},sk}=\frac{1}{2\pi}\cdot\left(\frac{1}{2}P_s(L_T)\right)^2\\&\quad\cdot\int_{-B_e}^{B_e}\sum_{k\neq s}\left|\widetilde{P}_k(0,\omega)\right|^2\left|H^{\text{XPM}}_{sk}(\omega)\right|^2d\omega\ \text{(Mark)}\\&\approx 0\quad\text{(Space)}\end{aligned} \quad (14)$$

where B_e is the signal bandwidth and $(1/2)P_s(L_T)$ is the average received optical power of channel s after a transmission distance L_T. Accordingly, the equivalent Q^2 due to XPM only can be written as

$$Q^2_{\text{XPM}}=\frac{4}{\frac{1}{2\pi}\int_{-B_e}^{B_e}\sum_{k\neq s}\left|\widetilde{P}_k(0,\omega)\right|^2\left|H^{XPM}_{sk}(\omega)\right|^2d\omega}. \quad (15)$$

We note that $H^{\text{XPM}}_{sk}(\omega)$ is a high-pass transfer function, which means the variance of XPM interference in (14) is higher if the modulation signal has higher bandwidth. Therefore, modulation schemes with smaller bandwidths (e.g., 2.5 Gb/s) are preferred to larger bandwidths (e.g., 10 Gb/s) from the viewpoint of minimizing XPM interference.

In conventional DWDM systems, one can assume that $\exp(-\alpha L)\ll 1$, and the modulation bandwidth is much smaller than the channel spacing, i.e., $\omega d^{(n)}_{sk}\gg\omega^2D^{(n)}_s\lambda^2_s/4\pi c$, then $b^{(n)}_s$ can be neglected and (11) can be simplified to (16) [17], shown at the bottom of the page. However, this assumption is not valid in U-DWDM systems, and the exact form (11) must be used in the following analysis.

C. Self-Phase Modulation and Residual Linear Dispersion

The analytical form for XPM interference can also be used to analyze SPM distortion. In (11), in the limiting case when $k=s$, the normalized frequency response of SPM distortion can be written as (17), shown at the bottom of the page. The distorted pulse waveform due to ISI and SPM can be approximated as

$$\begin{aligned}&\hat{P}_{\text{SPM},s}(L_T,t)\\&=\hat{P}_s(L_T,t)\cdot\left(1+\Delta\hat{P}_{\text{SPM},s}(L_t,t)\right)\\&=\hat{P}_s(L_T,t)\cdot\left(1+\frac{1}{2\pi}\int_{-B_e}^{B_e}\widetilde{P}_s(0,\omega)\cdot H^{\text{SPM}}_s(\omega)e^{j\omega t}d\omega\right).\end{aligned} \quad (18)$$

In (18), $\Delta\hat{P}_{\text{SPM},s}(L_T,t)$ is the waveform distortion due to the combination of SPM and linear dispersion (similar to what was derived for XPM in (12)). In our calculations in Section III, SPM-limited Q^2 ((1)) will be obtained by using the mean (m_1) and variance (σ_1) at the mark level of distorted waveform (obtained from (18) at the optimum sampling point) and neglect the contribution from space level (i.e., $\sigma_0\approx 0$). The waveform distortion at space due to linear dispersion is taken into account by replacing m_0 with the highest level at space, which causes EOP.

III. Overall System Limitations

In this section, we will calculate the overall U-DWDM system limitations by considering ISI, optical amplifier noise, and all the optical nonlinearities discussed previously. A generalized periodically amplified and dispersion-compensated U-DWDM system shown in Fig. 1(b) is used. We assume optical amplifier gain tilts are perfectly equalized, and DCFs are used for

$$H^{\text{XPM}}_{sk}(L_T,\omega)=\sum_{n=1}^{N}\left\{4\gamma^{(n)}_s\prod_{\ell=1}^{n-1}g^{(n)}_k\cdot\exp\left[\sum_{\ell=1}^{n-1}\left(-\alpha^{(\ell)}L^{(\ell)}+jd^{(\ell)}_{sk}\omega L^{(\ell)}\right)\right]\frac{\sin\left(B^{(n-1)}_s\right)}{a^{(n)}_{sk}}\right\}. \quad (16)$$

$$\begin{aligned}H^{\text{SPM}}_s(L_T,\omega)&=\left.\frac{1}{2}H^{\text{XPM}}_{sk}(L_T,\omega)\right|_{k=s}\\&=\sum_{n=1}^{N}\left\{\gamma^{(n)}_s\prod_{\ell=1}^{n-1}g^{(\ell)}_s\cdot\exp\left[\sum_{\ell=1}^{n-1}\left(-\alpha^{(\ell)}L^{(\ell)}\right)\right]\frac{2}{\left(\alpha^{(n)}\right)^2+\left(b^{(n)}_s\right)^2}\right.\\&\quad\left.\cdot\left[\alpha^{(n)}\sin\left(B^{(n-1)}_s\right)-b^{(n)}_s\cos\left(B^{(n-1)}_s\right)+\left[\alpha^{(n)}\sin\left(-B^{(n)}_s\right)-b^{(n)}_s\cos\left(B^{(n)}_s\right)\right]\exp\left(-\alpha^{(n)}L^{(n)}\right)\right]\right\}.\end{aligned} \quad (17)$$

broad-band dispersion and dispersion-slope compensation. A tunable PDC, with continuous tuning range up to -2000 ps/nm is used for individual channel performance optimization between linear dispersion and SPM/XPM. For simplicity, periodically amplified systems are assumed that have the same fiber length and DCR per span. We assume that the launched optical power into each transmission fiber span is equal, and the optical power into each DCF is 3 dB lower than the launched power to avoid additional nonlinearities generated in DCF. To focus on the fundamental system limitation due to optical fiber nonlinearities, we assumed an ideal rectangular optical filter whose bandwidth equals to channel spacing and a receiver whose electrical bandwidth equals to 0.8 times data rate. Numerical results are obtained by solving NLSE directly by using the split-step Fourier (SSF) method with a sampling rate of 2.56 THz and 2^{18} sample points (256 and 1024 symbols per channel per simulation for 2.5 and 10 Gb/s, respectively). The accuracy of the SSF method was confirmed by gradually reducing the step size. A maximum nonlinear phase change of 0.05 °/step was used in the numerical simulation. Q^2 is calculated directly from the sample mean and standard deviation of the simulated waveform at an optimum sampling point.

Solid and dotted curves in Fig. 3 show the calculated FWM- and ASE-limited fiber input powers per channel (at $Q^2(\text{ dB}) \geq 15.6$ dB) as a function of cascaded amplifier stages N, for 2.5-Gb/s/6.25-GHz systems in both NZDSF and SMF. An amplifier span length of 40 km was assumed. Three different DCRs—100, 90, and 60%—are shown to illustrate the effect of DCR on FWM. All symbols were obtained by choosing a specific input power/channel and running a simulation to obtain the maximum amplifier stages which can be cascaded to reach $Q^2(\text{ dB}) \geq 15.6$ dB. Simulation results include all fiber nonlinearity, linear dispersion, and ASE noise. Symbols near the interception points between ASE- and FWM-limited curves deviate away from their corresponding analytical FWM/ASE curves because in that region both FWM and ASE contribute to the combined Q^2 value (therefore Q^2 due to individual FWM or ASE may be a few decibels greater than 15.6 dB). We can see that FWM analytical results agree very well with numerical simulation results in 2.5-Gb/s/6.25-GHz systems in both types of fiber [(Fig. 3(a) for SMF and Fig. 3(b) for NZDSF]. Since numerical simulation results include all degradation factors, the results indicate that FWM is the dominant impairment in such systems. From Fig. 3, we can see that with DCR $= 100\%$, FWM-limited launched power in NZDSF is about 5 dB lower than that in SMF due to the lower local dispersion in NZDSF. We also observe that DCR $= 60\%$ offers the maximum transmission distance ($= 40$ km/stage $\times$ 115 stages) among the three cases in NZDSF. The transmission distances and optimum launched powers of 2.5-Gb/s/6.25-GHz systems in NZDSF ($D = 2$ ps/nm/km) are about 4600, 1600, and 900 km and -15, -20, and -22 dBm for 60, 90, and 100% DCR, respectively. Similarly, the numbers for 2.5-Gb/s/6.25-GHz systems in SMF are about 5200 and 1400 km and -13 and -18.5 dBm for 90 and 100% DCR, respectively.

From Fig. 3, we can see that for DCR $= 100\%$, the FWM-limited launched power is inversely proportional to N for both NZDSF and SMF. This is because with DCR $= 100\%$, FWM terms generated at every amplifier stage are added in-phase according to (3). Owing to the fact that phase matching is critical to the generation of FWM, maximum input power levels strongly depend on DCR. For DCR other than 100%, the relation between FWM interference and stage number is not simply amplitude addition ($\propto N^2$) or power addition ($\propto N$), but depends on the dispersion map of the system. The resultant FWM-limited maximum input power at a non-100% DCR can be much higher than that with 100% DCR, especially for a large number of cascaded amplifier stages. However, even though DCR other than 100% can effectively cause the residual dispersion to suppress FWM, it can also cause pulse broadening and enhance the PM-IM conversion via SPM and XPM (which is especially critical in 10-Gb/s systems). Therefore, there exists an optimum DCR for a U-DWDM system in which FWM is dominant. In contrast, 100% DCR is always the optimum point for a conventional DWDM system in which FWM is not the limiting factor.

From Fig. 3, we can see that as the number of cascaded amplifiers increases, the maximum FWM-limited input power decreases while the minimum ASE-limited input power increases. Therefore, the optimum fiber input power is a balance between FWM and ASE. With a launched power P per channel, we know from (8) that $Q^2_{\text{FWM}} \propto 1/P^2$. Let $Q^2_{\text{FWM}} = K_{\text{FWM}}/P^2$, where K_{FWM} is a constant for a fixed system at a certain transmission distance and can be calculated by (8). Similarly, we have $Q^2_{\text{ASE}} = K_{\text{ASE}} \cdot P$ for ASE noise (assuming signal–spontaneous beat noise dominate). In a U-DWDM system, where FWM is the dominant fiber nonlinearity, we have $\left(Q^2_{\text{total}}\right)^{-1} = \left(Q^2_{\text{ASE}}\right)^{-1} + \left(Q^2_{\text{FWM}}\right)^{-1}$, and the optimum launched power P_{opt} at a certain distance can be found by

$$\frac{d}{dP}\left[\left(\left(Q^2_{\text{ASE}}\right)^{-1}+\left(Q^2_{\text{FWM}}\right)^{-1}\right)^{-1}\right]=\frac{d}{dP}\left[\frac{1}{K_{\text{ASE}}P}+\frac{P^2}{K_{\text{FWM}}}\right] = 0. \tag{19}$$

Therefore, $P_{\text{opt}} = \sqrt[3]{1/2}\cdot P_{\text{eq}}$ or $P_{\text{opt}}(\text{dB}) \simeq P_{\text{eq}}(\text{ dB}) - 1$ dB, where $P_{\text{eq}} = \sqrt[3]{K_{\text{FWM}}/K_{\text{ASE}}}$ is the launched power level at which $Q^2_{\text{ASE}} = Q^2_{\text{FWM}}$. The relation between Q^2_{ASE} and Q^2_{FWM} when a system is optimized is $Q^2_{\text{ASE}}(\text{dB}) \simeq Q^2_{\text{FWM}}(\text{dB}) - 3$ dB. Furthermore, if we assume $Q^2_{\text{total}} = 15.6$ (dB) at the maximum transmission distance, we find $Q^2_{\text{ASE}}(\text{dB}) \simeq 17.5$ dB and $Q^2_{\text{FWM}}(\text{dB}) \simeq 20.5$ dB at the optimum launched power. Note that this general rule holds for any $Q^2_{\text{NLD}} \propto 1/\overline{P}_s^2$ (e.g., FWM, XPM, SPM, etc.). To show how the optimum launched power is found in a particular long-haul U-DWDM system, an example is illustrated in Fig. 4. We plot the Q^2 as a function of launched optical power in a 4640 km 2.5-Gb/s/6.25-GHz system using NZDSF fibers ($D = 2$ ps/nm/km), with 40 km per span and DCR $= 60\%$. In this case, FWM is the dominant nonlinearity, and the dotted line represents analytical results based on (8). As expected, the optimum launched power is a balance between ASE and FWM. The optimum launched power ($P_{\text{opt}} = -15$ dBm) is about 1 dB lower than the power ($P_{\text{eq}} = -14$ dBm) which gives $Q^2_{\text{ASE}} = Q^2_{\text{NL}}$. Also note that at $P_{\text{opt}} = -15$ dBm, $Q^2_{\text{ASE}}(\text{dB}) \simeq 17.5$ dB and $Q^2_{\text{NL}}(\text{dB}) \simeq 20.5$ dB, as expected.

Fig. 3 can be plotted in a different way, as shown in Fig. 5(a), to explicitly show that the maximum transmission distance in

an NRZ-modulated 2.5-Gb/s/6.25-GHz NZDSF system is obtained at optimum DCRs of about 40–60%. The maximum distance was calculated based on a received Q^2 of 15.6 dB. For every DCR, the input power per channel was swept from 0 to -25 dBm with a 0.5-dB step size to find the maximum achievable transmission distance. Because a typical NZDSF has a dispersion value ranging from 2–6 ps/nm/km, we analyzed both the upper limit ($D = 6$ ps/nm/km, dotted curves) and lower limit ($D = 2$ ps/nm/km, dashed curves), and use a solid curve to represent the worse of the two. The analytical and numerical results of maximum transmission distance for an 80-km span as a function of DCR are also shown in Fig. 5(a). We can see that there exists an optimum DCR of about 40–60% and 20–40% for 40- and 80-km spans, respectively, rather than $\sim 100\%$ in conventional DWDM systems. The maximum distances are about 4500 and 2300 km for 40- and 80-km spans, respectively. Also indicated in the same figure is the linear-dispersion limitation (dashed–dotted curve) at long wavelength ($D = 6$ ps/nm/km) and low DCR (DCR $< 50\%$) region and is given by [18]

$$R^2\left(\sum_{n=1}^{N} D^{(n)} \cdot L^{(n)} - \text{PDC}\right) < 104\,000 \left(\frac{\text{Gb}}{\text{s}}\right)^2 \cdot \left(\frac{\text{ps}}{\text{nm}}\right) \tag{20}$$

where R is the data rate in gigabits per second, $D^{(n)}$ is the fiber dispersion (in picoseconds/nanometers/kilometers) of stage n, $L^{(n)}$ is the fiber span length (in kilometers) of stage n, N is the total number of stages, and PDC represents the dispersion of a the postdispersion compensator [PDC $= -2000$ ps/nm in Fig. 5(a)].

Fig. 5(b) and (c) shows the corresponding calculated Q^2 of individual noise and interference terms. From Fig. 5(a)–(c), we can see that in a 2.5-Gb/s/6.25-GHz system, the optimum DCR is resulted from the tradeoff between linear dispersion and FWM. FWM is the dominant optical nonlinearity for all DCRs, especially in the short-wavelength region ($D = 2$ ps/nm/km). Note that $Q^2_{\text{ASE}} \approx 17.5$ dB and $Q^2_{\text{NLD}} \approx 20.5$ dB for all DCR $> 50\%$. The dashed–dotted curve shown in Fig. 5(b) is the sum of all nonlinearity and ASE noise. The difference between the dash-dotted and dotted curves is due to linear-dispersion-induced eye-opening penalty. Because we use (20) as linear-dispersion limitation, eye-opening penalty is kept below 1 dB. The dash-dotted curve is not shown in Fig. 5(c), because in this region, the linear-dispersion effect can be neglected.

Having discussed the maximum transmission distances of 2.5-Gb/s/6.25-GHz systems in NZDSF, we now turn to the cases of SMF, as shown in Fig. 6. Fig. 6(a) shows the linear-dispersion limitation with and without PDC. We can see that the effect of PDC on the optimum DCR and maximum distance is small. This can be understood by the fact that linear-dispersion-limited transmission distances (dotted curves) are much longer than the maximum transmission distance at the optimum DCR. The maximum transmission distance in SMF is about 900 and 2300 km longer than that in NZDSF for 40- and 80-km span length, respectively. Fig. 6(b) shows the calculated Q^2 of individual nonlinearity, linear dispersion, and ASE. The optimum DCR is around 85–93% [Fig. 6(a)], which is a tradeoff among FWM, SPM/XPM, and linear dispersion [Fig. 6(b)]. We can see that FWM dominates in the range

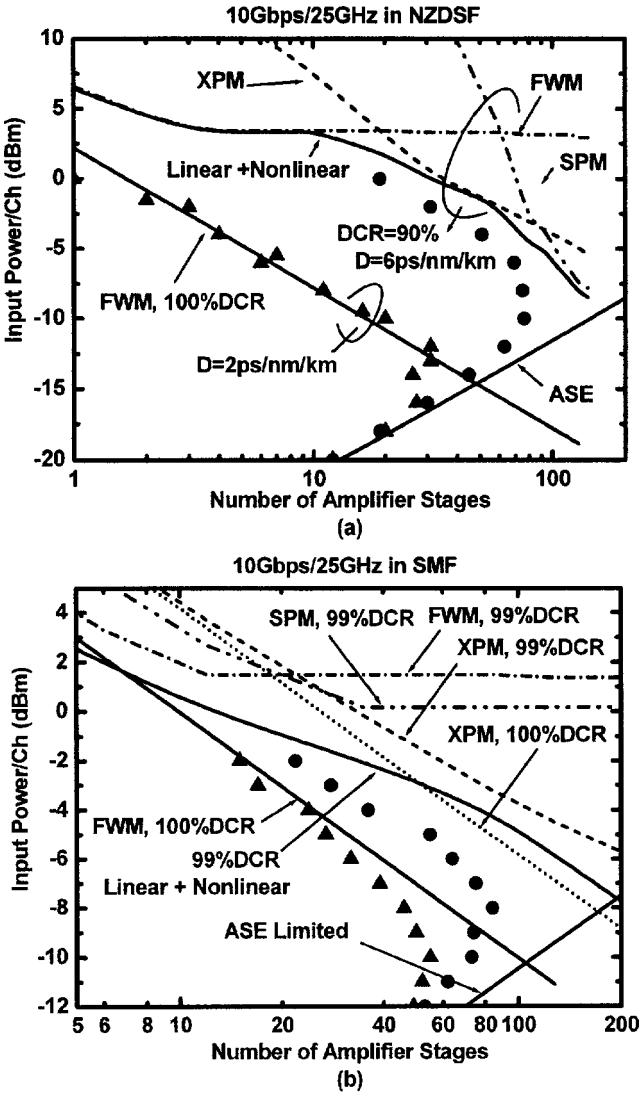

Fig. 8. Fiber input power per channel as a function of amplifier stages for different DCRs in a 10-Gb/s/25-GHz system, with 40 km per amplifier stage. Curves are calculation results, and symbols are numerical simulation results. (a) NZDSF: ▲: DCR $= 100\%$; •: DCR $= 90\%$; (b) SMF: ▲: DCR $= 100\%$; •: DCR $= 99\%$.

DCR $> 90\%$; SPM, XPM, and FWM must all be considered for DCR between 80 and 90%; linear dispersion dominates for DCR $< 80\%$.

Fig. 7 shows the optimum launched powers for different DCRs to achieve the maximum transmission distances given previously in Figs. 5 and 6 for NZDSF and SMF, respectively. Note that because of the stronger FWM in NZDSF, the optimum launched power levels in NZDSF are lower than those in SMF. The optimum launched power levels in NZDSF are -15 and -12 dBm at DCR $=$ 40–60% (40-km span) and 20–40% (80-km span), respectively. The optimum launched power levels in SMF are about -13 and -10 dBm at about 85–93% DCR for 40- and 80-km spans, respectively.

Fig. 8(a) and (b) shows fiber nonlinearities (including FWM, SPM, and XPM) and ASE-limited optical launched powers per channel for 10-Gb/s/25-GHz systems as a function of cascaded amplifier stages [Fig. 1(b)] in NZDSF and SMF, respectively.

Curves are calculated results based on (8), (15), and (18) for FWM, XPM, and SPM, respectively; discrete symbols are numerical simulation results, which include all fiber nonlinearities, linear dispersion, and ASE. Similar to Fig. 3, near the interception points of nonlinearity- and ASE-limited curves, symbols deviate away from calculated results because in these regions symbols include the contributions from both nonlinearity and ASE; therefore the input power for the ASE-limited case needs to be higher than that at $Q^2 = 15.6$ dB, and the input power for the nonlinearity-limited case needs to be lower than that at $Q^2 = 15.6$ dB. For ideal DCR $= 100\%$, it is always FWM limited, and XPM and SPM effects can be neglected. This is clear from the good match between simulation data (▲) and calculated FWM limitations with DCR $= 100\%$ in Fig. 8(a) and (b). We can see in Fig. 8(a) and (b) that XPM and SPM start to dominate over FWM after about 20 stages (800 km) for DCR $\neq 100\%$ in both NZDSF and SMF. As opposed to a 2.5-Gb/s/6.25-GHz system in which FWM is almost always the dominant limiting factor at optimum DCR, a 10-Gb/s/25-GHz system at an optimum DCR (e.g., 90% for NZDSF) must consider SPM, XPM, and FWM altogether.

Results shown in Fig. 8 are calculated (or simulated) with a tunable PDC before each receiver to optimize the individual 10-Gb/s channel performance. We found that there exists an optimum PDC (rather than compensating all residual dispersions) in cases where SPM or XPM cannot be neglected. Fig. 9(a) shows an example of the EOP due to SPM and linear dispersion as a function of PDC, in a 3600-km NZDSF ($D = 6$ ps/nm/km) with DCR $= 90\%$. The residual dispersion in such a transmission system is 2160 ps/nm. In the case of considering linear dispersion only (dashed curve and open symbols), the optimum PDC value is to completely compensate the residual dispersion accumulated from the non-100% DCR in every stage. However, in the case when SPM cannot be ignored in a 10-Gb/s/25-GHz system due to the large PDC-dispersion-induced PM-to-IM conversion, we can find that the optimum PDC is about -1200 ps/nm instead of -2160 ps/nm. Fig. 9(b) compares the eye diagrams obtained from calculations (using (18)) and numerical simulation. These results show that (18) can be used as a simple and effective method to evaluate the combined waveform distortion due to linear dispersion and SPM and, in turn, find the optimum PDC. In our calculations and simulations, this optimization of PDC value has always been implemented when SPM/XPM must be considered.

The maximum transmission distance of a 10-Gb/s/25-GHz NZDSF system is shown in Fig. 10(a). Similar to Fig. 5(a), maximum distance limitation in both $D = 2$ and 6 ps/nm/km regions are shown in the figure. We can see that the optimum DCR is quite different from those of 2.5-Gb/s/6.25-GHz systems in Fig. 5(a). This is because 10-Gb/s systems are much more sensitive to fiber dispersion, even though the larger channel spacing can reduce various fiber nonlinearity-induced impairments. The maximum transmission distance is about 3800 km and 3000 km with optimum DCRs of 90–95% and 86–91% for 40- and 80-km spans, respectively. Note that the optimum DCR is under the assumption that the PDC is capable of compensating any residual dispersion lower that 2000 ps/nm.

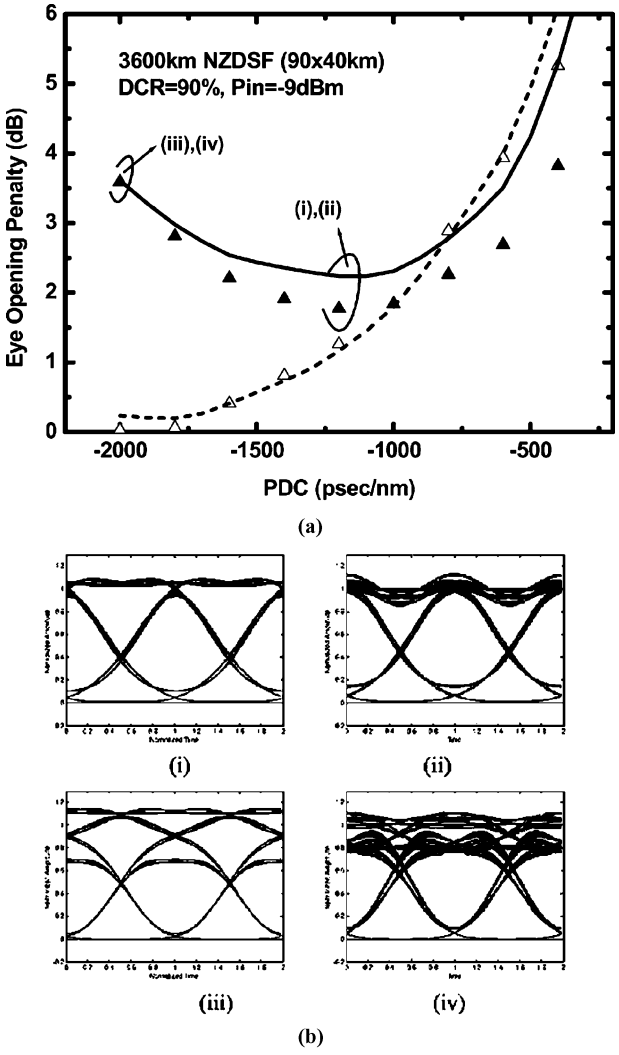

Fig. 9. Calculated and simulated eye-opening penalty (EOP) due to SPM and linear dispersion as a function of PDC. Assume a single-channel 10-Gb/s system over 3600 km of NZDSF fiber ($D = 6$ ps/nm/km). DCR $= 90\%$. (a) Solid and dashed curves are calculated EOPs due to SPM + linear dispersion and linear dispersion only, respectively. ▲ and △ are simulated EOPs due to SPM + linear dispersion and linear dispersion only, respectively. (b) Eye diagrams obtained via calculations (i) and (iii) and simulations (ii) and (iv).

In Fig. 10(a), the linear-dispersion limitations (dashed–dotted curves) are calculated in the long-wavelength region ($D = 6$ ps/nm/km). We notice that when there is no PDC applied, two negative impacts are incurred. The first is that the maximum transmission distance is reduced to about 3000 (from 3800) and 2200 (from 3000) km for 40- and 80-km span, respectively. The second is that the optimum DCR for both spans is narrowed down to a sharp range of about 96%, as opposed to the original 90–95% range when the -2000-ps/nm PDC was used. This sharp range of optimum DCR is not practical in real-world systems. Fig. 10(b) shows the corresponding Q^2 for individual limiting factors in the short-wavelength region ($D = 2$ ps/nm/km) for DCR $\geqq 91\%$ and long-wavelength region ($D = 6$ ps/nm/km) for DCR $\leqq 90\%$. We find that the dominant fiber nonlinearities are XPM and SPM in the higher dispersion region and FWM in the lower dispersion region.

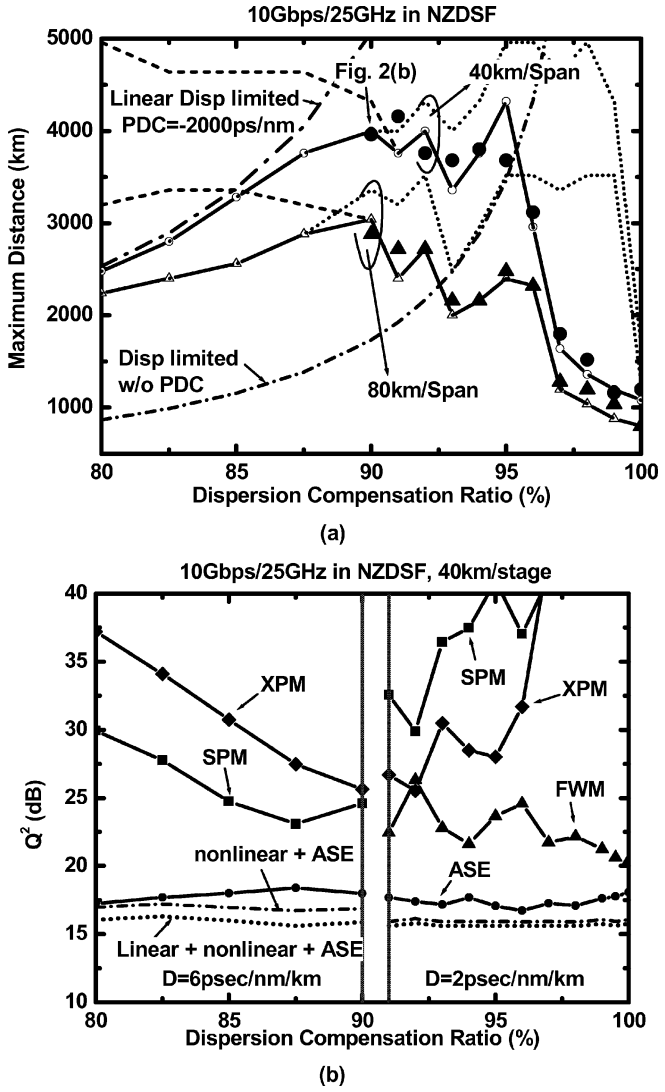

Fig. 10. (a) Calculated and simulated fiber linear-dispersion- and fiber nonlinearity-limited maximum transmission distance of a 10-Gb/s/25-GHz system ($Q^2 = 15.6$ dB) as a function of inline DCR in NZDSF. Solid curves are analytical results for 40- and 80-km fiber spans with dashed and dotted curves for $D = 2$ and 6 ps/nm/km, respectively. • and ▲ are simulation results with 40- and 80-km fiber span, respectively. Inline DCFs are used for dispersion compensation, and the input power into DCF is 3 dB lower than that into transmission fiber. A tunable PDC (up to -2000 ps/nm) was used to optimize the individual channel performance. (b) Calculated corresponding individual Q^2 of 40-km fiber span. The results shown are calculated with $D =$ 6 and 2 ps/nm/km for DCR $\leqq 90\%$ and DCR $\geqq 91\%$, respectively.

Fig. 11(a) shows the transmission system performance of 10-Gb/s/25-GHz system in SMF. The calculated and simulated maximum distances are obtained with a -2000-ps/nm tunable PDC to optimize system performance. The optimum DCR for 10-Gb/s/25-GHz systems in SMF is 98–99% because of the larger fiber dispersion. Note that in this case, the optimum DCR range is already very narrow. When no PDC is used, shown by the dotted line without PDC in Fig. 11(a), this range will be even narrower. Fig. 11(b) and (c) shows the individual Q^2 due to various impairments for 40- and 80-km spans, respectively. We can see that SPM and XPM are the two main limiting fiber nonlinearities in a 10-Gb/s/25-GHz system in SMF. For DCR $< 90\%$, the transmission distances are limited by linear dispersion.

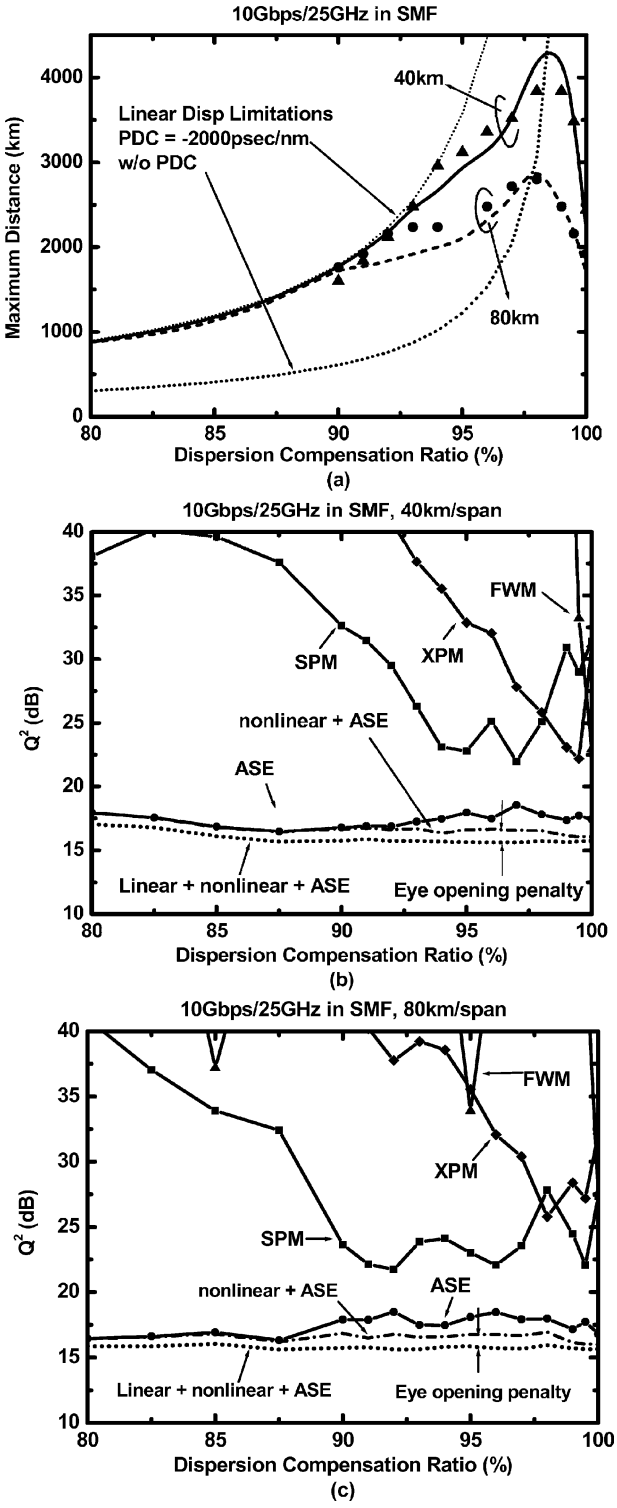

Fig. 11. (a) Calculated and simulated fiber linear-dispersion- and nonlinearity-limited maximum transmission distance of 10-Gb/s/25-GHz systems ($Q^2 \geqq 15.6$ dB) as a function of inline DCR in SMF. Solid and dashed curves are analytical results for 40 and 80 km, respectively. • and ▲ are simulation results with 40- and 80-km fiber spans, respectively. Inline DCFs are used for dispersion compensation, and the input power into DCF is 3 dB lower than that into transmission fiber. A tunable PDC (up to -2000 ps/nm) was used to optimum the individual channel performance. (b) and (c) Calculated corresponding individual Q^2 of 40- and 80-km fiber span, respectively.

Fig. 12 shows the calculated optimum PDC [corresponding to the maximum distances in Figs. 10(a) and 11(a)] as a

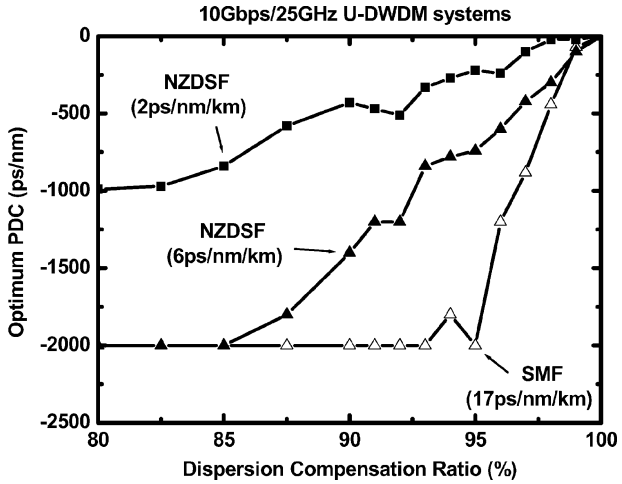

Fig. 12. Calculated optimum PDC as a function of dispersion compensation ratio at the optimum transmission distances in Figs. 10(a) and 11(a).

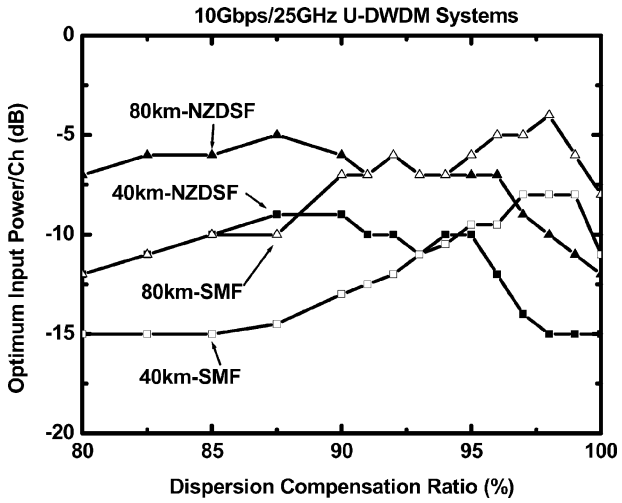

Fig. 13. Optimum launched power per channel as a function of DCR, corresponding to the maximum transmission distances at the various DCRs in Figs. 9(a) and 10(a).

function of DCR. In our calculations and simulations, we assumed that the maximum PDC is up to -2000 ps/nm. From (20), a PDC can increase the transmission distance by $\Delta L = \text{PDC}/(D \cdot (1 - \text{DCR}))$ for a system limited by linear dispersion (i.e., in the region DCR < 95 and 85% for SMF and $D = 6$ ps/nm/km NZDSF, respectively). However, when a system is limited by fiber nonlinearity instead, increasing PDC is not going to be useful (i.e., in the region DCR > 95 and 85% for SMF and $D = 6$ ps/nm/km NZDSF, respectively). Judging from Figs. 10(a) and 11(a), which show that the optimum DCRs are about 90–95% and 98–99% for NZDSF and SMF, respectively, -2000-ps/nm PDC is quite sufficient for both types of fibers.

Fig. 13 shows the optimum launched power per channel of 10-Gb/s/25-GHz systems in both NZDSF and SMF. The optimum launched powers in NZDSF are about -10 and -6 dBm (at DCR $= 95$ and 90%) for 40- and 80-km spans, respectively. The optimum lunched powers in SMF are about -8 and -4 dBm (at DCR $= 99$ and 98%) for 40- and 80-km spans, respectively.

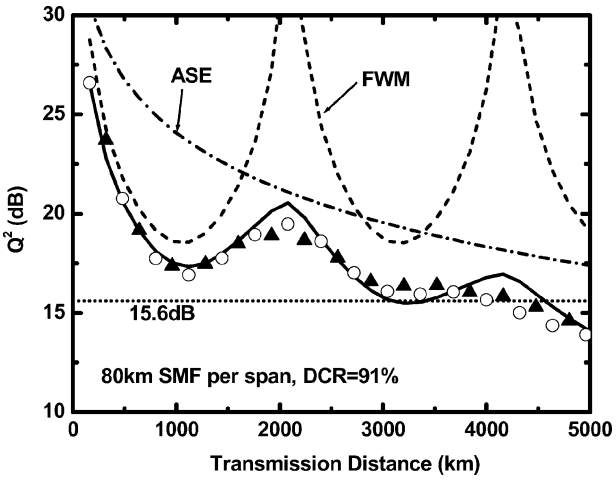

Fig. 14. Q^2 as a function of transmission distance when FWM and ASE dominate. Assume a 2.5-Gb/s/6.25-GHz system in SMF with span $= 80$ km and DCR $= 91\%$. Curves are analytical results for Q^2_{FWM} (dashed), Q^2_{ASE} (dash–dotted), and $Q^2_{\text{FWM+ASE}}$ (solid). ▲ and ◯ are simulation results with SSF method and with commercial simulation software (VPI-TransmissionMaker), respectively.

IV. Discussion

The results obtained in this work are based on the assumption of being able to use ideal rectangular optical filters. However, it is well known that filter shape and bandwidth have significant effect on ISI and adjacent channel interference, especially in U-DWDM systems [5], [19]. Furthermore, when the interplay between filters and fiber nonlinearities are considered, the problem becomes even more complicated, and no analytical forms are yet available for system optimizations [9]. Therefore, more investigations need to be carried out to understand the optimum filter design for U-DWDM systems.

One may find that the calculated maximum transmission distances in Section III are shorter than some published experiment results [2], [3]. The main difference is because $Q^2 = 15.6$ dB was used in all calculations in this work, which leaves a reasonable margin for practical system operation with FEC [e.g., a 5-dB coding gain for typical RS(255 239)]; while in most previous experiments, the transmission distances were pushed to the limit with a more powerful FEC and without any operating margin. Second, in our calculations, all channels were assumed to have the same polarization, while polarization interleaving was used in most published experiments. Polarization interleaving can reduce fiber nonlinearity-induced interference between channels; therefore, the net effect of a polarization-interleaved DWDM system with Δf channel spacing will be equivalent to the case of a channel spacing between Δf and $2\Delta f$. Nevertheless, we believe the assumptions used in this paper fit practical system conditions better.

An interesting phenomenon we found is that Q^2 of U-DWDM systems is not always monolithically decreasing as a function of distance because of the resonance effect of FWM [11]. The FWM resonance can be illustrated with Fig. 14. Fig. 14(a) shows calculated and simulated Q^2 as a function of transmission distance in a 2.5-Gb/s/6.25-GHz system with an 80-km SMF span and 91% DCR [corresponding to the maximum distance point

TABLE II
SUMMARY OF OPTIMUM LAUNCH POWER PER CHANNEL UNDER DIFFERENT SYSTEM CONDITIONS

	Span Length	SMF	NZDSF
2.5Gbps/6.25GHz	40km	-13dBm/ch (+15dBm/640ch) @DCR=85-93%	-15dBm/ch (+13dBm/640ch) @DCR=40-60%
	80km	-10dBm/ch (+18dBm/640ch) @DCR=85-93%	-12dBm/ch (+16dBm/640ch) @DCR=20-40%
10Gbps/25GHz	40km	-8dBm/ch (+14dBm/160ch) @DCR=98-99%	-10dBm/ch (+12dBm/160ch) @DCR= 90-95%
	80km	-4dBm/ch (+18dBm/160ch) @DCR=98%	-6dBm/ch (+16dBm/160ch) @DCR= 86-91%

TABLE III
SUMMARY OF MAXIMUM TRANSMISSION DISTANCE UNDER DIFFERENT SYSTEM CONDITIONS

	Span Length	SMF	NZDSF
2.5Gbps/6.25GHz	40km	5400km (SPM,XPM,FWM) @DCR= 85-93%	4500km (FWM) @DCR=40-60%
	80km	4600km (SPM,XPM,FWM) @DCR=85-93%	2300km (FWM) @DCR=20-40%
10Gbps/25GHz	40km	4300km (XPM) @DCR=98-99%	3800km (FWM) @DCR= 90-95%
	80km	2800km (XPM) @DCR=98%	3000km (FWM) @DCR= 86-91%

in Fig. 6(a)]. From the calculation, we know that the Q^2 is dominated by ASE and FWM. According to (3), the resonance period of FWM in a periodically amplified DWDM system can be calculated by

$$\Delta\beta \cdot (1 - \mathrm{DCR}) \cdot N \cdot L = 2\pi \ (\mathrm{DCR} \neq 100\%). \qquad (21)$$

Equation (21) means the phase of FWM interference generated in the N amplifier stages is equally distributed over 0 to 2π, which minimizes the added phasor in (3). Using (21), we can get a period of $N \cdot L \simeq 2089$ km, as shown in the Fig. 14. The calculated and simulated results were double-checked by a commercial optical system simulation software (VPI-TransmissionMaker), and the results show a good match with both our analysis and simulation. We find that the simulation results do not have resonance peaks as strong as those of analytical results, especially after a long transmission distance. This is because the analytical solutions are derived by CW FWM with a probability of coexisting marks; while in the real system, the NRZ-modulated signal has a $\pm$2.5-GHz frequency spread around the center wavelength, which randomizes the phasor in each amplifier stage slightly (e.g., $\Delta\beta^{(\ell)} \approx 0.008$ rad/km in Section II-A can be varied slightly to $\Delta\beta^{(\ell)} \approx 0.004 \sim 0.014$ rad/km). Nevertheless, we can see the simulation results match very well with analytical results. It should be cautioned that, due to this resonance effect, there is a wide range of transmission distance that exhibits a Q^2 value close to 15.6 dB (e.g., from 3000–4000 km in Fig. 14). Therefore, using $Q^2 = 15.6$ dB as a hard cutoff criterion to find the maximum transmission distance may not be quite appropriate in this case.

V. CONCLUSION

We have analytically and numerically investigated the transmission performance of 2.5- and 10-Gb/s U-DWDM systems with a spectral efficiency of 0.4 b/s/Hz. Numerical simulations confirmed that the transmission system performance can be accurately predicted by using analytical equations for individual optical nonlinearity in both conventional SMF and NZDSF (e.g., LEAF or TrueWave fiber). The optimum launched power, the maximum transmission distance with dominant nonlinearities, and the corresponding DCR in various systems are summarized in Tables II and III, respectively. Generally speaking, the optimum launched power is higher and the maximum distance is longer in SMF than those in NZDSF. We observe that in

all U-DWDM systems, there exists an optimum DCR range to reach a maximum transmission distance. Most systems have a relatively manageable DCR range, except for 10-Gb/s/25-GHz SMF system whose optimum DCR range is so narrow that it may be impractical in real-world systems. We also note that due to the dispersion-sensitive nature of 10-Gb/s/25-GHz systems, postdispersion compensation is required not only to increase the transmission distance, but also to increase the optimum DCR range. Table III also summarizes the dominant fiber nonlinearity under different system conditions. We see that in NZDSF, FWM is always the dominant nonlinearity at the optimum DCR. In SMF, however, SPM, XPM, and FWM are all important nonlinearity impairments to consider in 2.5-Gb/s/6.25-GHz systems; and XPM is the dominant nonlinearity in 10-Gb/s/25-GHz systems at the optimum DCR.

APPENDIX

In the presence of waveform distortions due to fiber nonlinearities and/or linear dispersion, marks and spaces are split into several rails. Gaussian noise is superimposed on these rails. We assume marks and spaces are split into N_1 and N_0 rails, respectively. The levels are defined as $m_{j,0}, m_{j,1}, \ldots, m_{j,Nj-1}$ with probability of occurrence of $m_{j,k}$ set to be $p_{j,k}$ (where k stands for the kth rail). $j = 1$ (mark) or 0 (space). In the presence of waveform distortions, BER can be obtained from [7], [10] with decision threshold $m_{\rm th}$

$$P_e(m_{\rm th}) = \sum_{k=0}^{N_0-1} P_{0,k}(m_{\rm th}) + \sum_{k=0}^{N_1-1} P_{1,k}(m_{\rm th}) \qquad \text{(A1)}$$

where

$$P_{0,k}(m_{\rm th}) = \frac{p_{0,k}}{4}\text{erfc}\left(\frac{m_{\rm th} - m_{0,k}}{\sqrt{2}\sigma_{0,k}}\right) \qquad \text{(A2)}$$

and

$$P_{1,k}(m_{\rm th}) = \frac{p_{1,k}}{4}\text{erfc}\left(\frac{m_{1,k} - m_{\rm th}}{\sqrt{2}\sigma_{1,k}}\right). \qquad \text{(A3)}$$

REFERENCES

[1] H. Suzuki, M. Fujiwara, N. Takachio, K. Iwatsuki, T. Kitoh, and T. Shibata, "12.5-GHz spaced 1.28 Tb/s (512-channel × 2.5 Gbps) super-dense WDM transmission over 320-km SMF using multiwavelength generation technique," *IEEE Photon. Technol. Lett.*, vol. 14, pp. 405–408, Mar. 2002.

[2] G. Vareille, F. Pitel, and J. F. Marcerou, "3 Tbit/s (300 × 11.6 Gbit/s) transmission over 7380 km using C+L band with 25 GHz channel spacing and NRZ format," in *Proc. Optical Fiber Communications Conf. (OFC 2001)*, vol. 4, 2001, Postdeadline Paper PD22 -P1-3.

[3] C. R. Davidson, C. J. Chen, M. Nissov, A. Pilipetskii, N. Ramanujam, H. D. Kidorf, B. Pedersen, M. A. Mills, C. Lin, M. I. Hayee, J. X. Cai, A. B. Puc, P. C. Corbett, R. Menges, H. Li, A. Elyamani, C. Rivers, and N. S. Bergano, "1800 Gbps transmission of one hundred and eighty 10 Gbps WDM channels over 7,000 km using the full EDFA C-band," in *Proc. Optical Fiber Communications Conf. (OFC 2000)*, 2000, Postdeadline Paper PD25.

[4] L. Leng, S. Stulz, B. Zhu, L. E. Nelson, B. Edvold, L. Gruner-Nielsen, S. Radic, J. Centanni, and A. Gnauck, "1.6 Tb/s (160 × 10.7 Gbps) transmission over 4000 km of nonZERO dispersion fiber at 25-GHz channel spacing," *IEEE Photon. Technol. Lett.*, vol. 15, pp. 1153–1155, Aug. 2003.

[5] S. B. Jun, K. J. Park, and Y. C. Chung, "Transmission of 2.5-Gbps WDM channels spaced at 5 GHz over 480 km of single-mode fiber," *IEEE Photon. Technol. Lett.*, vol. 15, pp. 1309–1311, September 2003.

[6] K. Inoue, K. Nakanishi, K. Oda, and H. Toba, "Interference and power penalty due to fiber four-wave mixing in multichannel transmissions," *J. Lightwave Technol.*, vol. 12, pp. 1423–1439, Aug. 1994.

[7] S. Norimatsu and M. Maruoka, "Accurate Q-factor estimation of optically amplified systems in the presence of waveform distortions," *J. Lightwave Technology*, vol. 20, pp. 19–27, Jan. 2002.

[8] T. Mizuochi, K. Ishida, T. Kobayashi, J. Abe, K. Kinjo, K. Motoshima, and K. Kasahara, "A comparative study of DPSK and OOK WDM transmission over transoceanic distances and their performance degradations due to nonlinear phase noise," *J. Lightwave Technology*, vol. 21, pp. 1933–1943, Sept. 2003.

[9] H. Louchet, A. Hodzic, and K. Petermann, "Analytical model for the performance evaluation of DWDM transmission systems," *IEEE Photon. Technol. Lett.*, vol. 15, pp. 1219–21, Sept. 2003.

[10] C. J. Anderson and J. A. Lyle, "Technique for evaluating system performance using Q in numerical simulations exhibiting intersymbol interference," *Electron. Lett.*, vol. 30, pp. 71–72, Jan. 1994.

[11] D. Schadt, "Effect of amplifier spacing on four-wave mixing in multichannel coherent communications," *Electron. Lett.*, vol. 27, pp. 1805–1807, Sept. 1991.

[12] K. O. Hill, D. C. Johnson, B. S. Kawasaki, and R. I. MacDonald, "CW three-wave mixing in single-mode optical fibers," *J. Appl. Phys.*, vol. 49, pp. 5090–5106, 1978.

[13] N. Shibata, R. P. Braun, and R. G. Waarts, "Phase-mismatch dependence of efficiency of wave generation through four-wave mixing in a single-mode optical fiber," *IEEE J. Quantum Electron.*, vol. QE-23, pp. 1205–1210, July 1987.

[14] M. Eiselt, "Limits on WDM systems due to four-wave mixing: A statistical approach," *J. Lightwave Technol.*, vol. 17, pp. 2261–2267, Nov. 1999.

[15] A. Cartaxo, "Cross-phase modulation in intensity modulation-direct detection WDM systems with multiple optical amplifiers and dispersion compensators," *J. Lightwave Technol.*, vol. 17, pp. 178–190, Feb. 1999.

[16] E. Peral, W. K. Marshall, and A. Yariv, "Precise measurement of semiconductor laser chirp using effect of propagation in dispersion fiber and application to simulation of transmission through fiber grating," *J. Lightwave Technol.*, vol. 16, pp. 1874–1880, Oct. 1998.

[17] R. Hui, K. R. Demarest, and C. T. Allen, "Cross-phase modulation in multispan WDM optical fiber systems," *J. Lightwave Technol.*, vol. 17, pp. 1018–1026, June 1999.

[18] A. R. Chraplyvy and R. W. Tkach, "Treabit/second transmission experiments," *IEEE J. Quantum Electron.*, vol. 34, pp. 2103–2108, Sept. 1998.

[19] I. Lyubomirsky, T. Qui, J. Roman, M. Nayfeh, M. Y. Frankel, and M. G. Taylor, "Interplay of fiber nonlinearity and optical filtering in ultradense WDM," *IEEE Photon. Technol. Lett.*, vol. 15, pp. 147–149, Jan. 2003.

[20] T. Tsuritani, A. Agata, I. Morita, K. Tanaka, and N. Edagawa, "Performance comparison between DSB and VSB signals in 20 Gbit/s-based ultra-long-haul WDM systems," in *Optical Fiber Communications (OFC 2001) Tech. Dig.*, 2001, Paper MM5.

Mingchia Wu was born in Taichung, Taiwan, R.O.C., in 1973. He received the M.S. and Ph.D. degrees from the National Chiao-Tung University Hsinchu, Taiwan, in 1997 and 2004, respectively.

He was with OpVista, Inc., Irvine, CA, from 2000 to 2001, where he worked on ultra-dense-wavelength-division-multiplexed (DWDM) transmission system design. In 2002, he became a Research and Development Manager of the Optical Transceiver Department of Delta Electronics, Inc. His research interests are optical fiber nonlinear limitations in both subcarrier-multiplexed CATV systems and ultra-DWDM systems.

Winston I. Way (S'82–M'82–SM'88–F'01) received the M.S. and Ph.D. degrees from the University of Pennsylvania, Philadelphia, in 1981 and 1983, respectively.

He was with Applied Research, Bellcore (now Telcordia), Red Bank, NJ, from 1984 to 1992, where he pioneered research in subcarrier-multiplexed lightwave systems and conducted a number of well-known dense-wavelength-division-multiplexing (DWDM) digital/analog video transmission experiments. From 1992 to 2000, he was a Professor at the National Chiao-Tung University, Hsinchu, Taiwan, R.O.C., where he continued leading many research projects in HFC systems and networks. From 1998 to 2000, he was also a Consultant at Telcordia, conducting research on next-generation Internet optical networks. In 2000, he founded OpVista Inc., Irvine, CA, and has been developing ultra-DWDM transmission equipment. He is the author of the book *Broadband Hybrid/Fiber Coax System Technologies* (New York: Academic, 1998), has published more than 100 journal and conference papers, and holds more than a dozen published or pending U.S. patents.

Dr. Way has served on the technical program committees of OFC, MTT, OECC, the IEEE Lasers & Electro-Optics Society (LEOS), and the Optical Society of America (OSA).